

X-ray Microscopy Studies of Protein Adsorption on a Phase-Segregated Polystyrene/Polymethyl Methacrylate Surface. 1. Concentration and Exposure-Time Dependence for Albumin Adsorption

Li Li,[†] Adam P. Hitchcock,^{*,†} Nicholas Robar,^{†,‡} Rena Cornelius,[‡] John L. Brash,^{†,‡,§} Andreas Scholl,^{||} and Andrew Doran^{||}

BIMR, McMaster University, Hamilton, ON, Canada L8S 4M1, Chemical Engineering, McMaster University, Hamilton, ON, Canada L8S 4L7, School of Biomedical Engineering, McMaster University, Hamilton, ON, Canada L8S 4K1, and Advanced Light Source, Berkeley Lab, Berkeley, California 94720

Received: April 20, 2006; In Final Form: June 26, 2006

X-ray photoemission electron microscopy using synchrotron radiation illumination has been used to measure the spatial distributions of albumin on a phase-segregated polystyrene/poly(methyl methacrylate) (PS/PMMA) polymer thin film following adsorption from unbuffered, deionized aqueous solutions under a range of solution concentrations and exposure times. Chemical mapping of the albumin, PS, and PMMA shows that the distribution of albumin on different adsorption sites (PS, PMMA, and the interface between the PS and PMMA domains) changes depending on the concentration of the albumin solution and the exposure time. The preferred sites of absorption at low concentration and short exposure are the PS/PMMA interfaces. Albumin shows a stronger preference for the PS domains than the PMMA domains. The exposure-time dependence suggests that a dynamic equilibrium between albumin in solution and adsorbed on PS domains is established in a shorter time than is required for equilibrating albumin between the solution and the PMMA domains. The explanation of these preferences in terms of possible adsorption mechanisms is discussed.

1. Introduction

Protein adsorption on solid surfaces is a very complex process that depends on various interactions between protein and substrate, as well as the state of hydration of the protein and the surface, the structure of the protein, and the presence of other components such as buffer salts, coadsorbed species.¹ Understanding and controlling protein adsorption is an important issue in biomaterials since it is known that protein adsorption is the first event in the interaction of tissue with a material. Different techniques have been used to study protein adsorption, including Fourier transform infrared spectroscopy (FTIR),² surface plasmon resonance (SPR),^{3–5} ellipsometry,^{5,6} atomic force microscopy (AFM),^{7,8} surface matrix-assisted laser desorption ionization mass spectrometry (MALDI-MS),⁹ secondary ion mass spectrometry (SIMS),^{10,11} X-ray photoelectron spectroscopy (XPS),^{12,13} quartz crystal microbalance (QCM),^{14,15} and radiolabeling.¹⁶ While these techniques provide good analytical sensitivity, in many cases they do not provide chemically specific identification, and in others, they are not able to visualize and thus locate sites of protein adsorption on laterally heterogeneous surfaces. AFM has excellent spatial resolution but only limited chemical sensitivity. SIMS combines both chemical identification and mapping, but its spatial resolution is currently of the order of 1 μm . In many biomaterials applications a major effort is underway to control protein

adsorption by structuring and/or chemical patterning the surface at a sub-micrometer scale.^{17–19} Analytical tools such as that described in this work can provide useful feedback to assist such developments. At a more fundamental level, it is of interest to understand protein–surface interactions in more detail, particularly as related to the role of surface properties such as hydrophobicity and chemical functionality. The use of surfaces that present distinct regions having different surface properties in close proximity gives the possibility to investigate the effect of these properties “simultaneously” in a single material, on a competitive basis. Adsorption site preference on such surfaces is of interest from both kinetic and thermodynamic viewpoints. A kinetics perspective raises questions such as location of first attachment and the evolution of regional preference over time as the surface fills. This has been studied previously with much more limited spatial sensitivity using protein adsorption on surfaces with a compositional and thus hydrophobicity gradient.^{20,21} In this work the ability of X-ray spectromicroscopy to map protein distributions relative to surface domains at high resolution is used to study competitive adsorption on a chemically heterogeneous surface.

Recently, we demonstrated that synchrotron-based soft X-ray microscopy techniques can provide the required combination of chemical sensitivity, spatial resolution, and surface sensitivity. Specifically, we have shown that scanning transmission X-ray microscopy (STXM) can detect protein on complex polymer surfaces, both in the dried state and fully hydrated state.²² We have also shown that X-ray photoemission electron microscopy (X-PEEM) can map polymer surfaces at high spatial resolution (~ 80 nm).²³ X-PEEM was shown to be capable of identifying preferred sites of fibrinogen attachment at submonolayer levels

* Corresponding author. Tel.: 905-525-9140 ext. 24749. Fax: 905-521-2773. E-mail: aph@mcmaster.ca.

[†] BIMR, McMaster University.

[‡] Chemical Engineering, McMaster University.

[§] School of Biomedical Engineering, McMaster University.

^{||} Advanced Light Source, Berkeley Lab.

[‡] Summer student from Department of Biology, Mount Allison University, Sackville, NB, Canada.

on a phase-segregated polystyrene/poly(methyl methacrylate) (PS/PMMA) blend surface.²⁴

Here we report the first of a series of papers describing a systematic investigation by X-PEEM and STXM of the adsorption of human serum albumin (HSA) on the surface of a PS/PMMA blend at different conditions of concentration, exposure time, pH, temperature, ionic strength, and competitive adsorption. This first paper focuses on methodological issues, and the use of X-PEEM to probe the location of HSA on the PS/PMMA blend surface when adsorbed from deionized water solutions of various concentrations and after different exposure times.

2. Experimental Section

2.1. Materials. **2.1.1. Substrate.** PS (MW = 1.07 M, $\delta = 1.06$) and PMMA (MW = 312 K, $\delta = 1.01$) were obtained from Polymer Source Inc. and were used without further purification. A 30:70 w/w PS/PMMA (1 wt %) toluene (Aldrich, 99.8% anhydrous) solution was spun cast (4000 rpm, 40 s) onto clean 0.8×0.8 cm native oxide Si wafers (111) (Wafer World, Inc.), which had previously been degreased with trichloroethylene (Aldrich, +99.5% pure), acetone (Burdick & Jackson, HPLC grade), and methanol (Caledon), and then rinsed under running deionized water. The PS:PMMA/Si substrates were annealed at 160 °C for 12 h in a vacuum oven at a pressure of $\sim 10^{-4}$ Torr. Noncontact mode atomic force microscopy (AFM) measurements were used to measure the thickness of the PS:PMMA polymer film. The step height in the region of a fine scratch showed the film to be 40–50 nm thick. The discrete domains are ovoid PMMA islands with 500–800 nm width, separated by a similarly sized continuous domain of PS. Both the PS and PMMA domains also contain microdomains at the 10–200 nm size scale, amounting to $\sim 20\%$ of the majority domain. It is not clear why the minority PS component (30 wt %) forms the continuous domain, but the same morphology is observed for this type of spun-coat sample over a range of PS/PMMA compositions and molecular weights.²³

2.1.2. Albumin. Human serum albumin (HSA) was obtained from Behringwerke AG, Marburg, Germany, and found to be homogeneous as judged by sodium dodecyl sulfate polyacrylamide gel electrophoresis (SDS-PAGE). All the albumin solutions used in this work were prepared from deionized (DI) water. The 0.005, 0.01, and 0.05 mg/mL albumin solutions were prepared by successive dilution from a 0.1 mg/mL albumin stock solution. Albumin is highly soluble and does not denature in deionized water unless heated above 70 °C and under strong alkaline conditions.²⁵ The pH of the unbuffered albumin solutions was measured to be 7.2 ± 0.2 , slightly more acidic than physiological pH. We have also studied the adsorption of albumin from phosphate saline buffer (PSB) solutions. It is well-known that the change in ionic strength of a solution will affect the range of electrostatic interactions. Indeed, as will be presented elsewhere, changing from deionized water to PSB leads to some differences in the adsorption site preferences for albumin, although smaller than those found in our previous study on fibrinogen adsorption.²⁴ We present these results for adsorption from DI water as a base for comparison to the other aspects of this extended study.

2.2. Protein Exposure. To prepare samples for the concentration-dependence study, three wells of a Fisher multiwell plate (1 cm diameter well) were filled with albumin solutions of different concentrations. The remaining wells were filled with deionized water. A piece of the PS/PMMA/Si substrate was introduced into each albumin solution and then the plate was shaken gently in the horizontal direction to expel any air bubbles

that may have formed on the substrate surfaces. After 20 min exposure, each substrate was taken out of the albumin solution and incubated in fresh deionized water in another well. After 2 min, the substrate was moved to another cell with fresh deionized water. This washing procedure was repeated four times for each substrate. The albumin-covered PS/PMMA sample was then removed from the final well and dried by carefully touching the edge of the Si wafer with lens paper. For the exposure-time-dependence study, the PS/PMMA sample was exposed to a 0.01 mg/mL albumin solution for times of 5, 20, and 60 min.

2.3. X-PEEM. The X-PEEM (PEEM2) at ALS bending magnet beamline 7.3.1²⁶ was used for this study. The principles and performance of the instrument have been presented extensively elsewhere.²⁶ A schematic of the instrument is given in Figure 1 of ref 23. Briefly, the sample is illuminated by monochromatic X-rays, and the photoejected electrons are extracted into an electrostatic imaging column by a high electric field between the sample and the objective lens and transported with controlled magnification to a CCD camera. From the perspective of X-ray absorption, X-PEEM is a variant of the total electron yield method, which strongly emphasizes low kinetic energy secondary electrons. The sampling depth ($1/e$) of X-PEEM for polymers has been measured as 4 nm,²⁷ with signals effectively being integrated over the outer 10 nm of the sample. In this work, the light employed was elliptically polarized with 70–80% right circularly polarized light. The electrostatic field at the sample was 9 kV/mm. The projector voltage was then adjusted such that the resulting field-of-view was between 40 and 60 μm .

Image sequences²⁸ at the C 1s edge were recorded from several different areas of the sample and analyzed using techniques described below to derive quantitative maps of the PS, PMMA, and HSA distributions. In contrast to X-PEEM of hard materials, there are many challenges of X-PEEM measurements of radiation-sensitive organic soft matter. Since the previous X-PEEM work on PS/PMMA²³ and fibrinogen-covered PS/PMMA,²⁴ we have optimized sample preparation, data acquisition, and data analysis procedures extensively. The PS:PMMA layer is kept thin (< 50 nm) and flat (~ 10 nm rms) in order to avoid discharges. A 100 nm thick Ti filter is used to reduce second-order light in the C 1s region. The radiation damage rates for all three components have been characterized.²⁷ To reduce radiation exposure, a fast shutter has been implemented which, when used to blank the beam between successive data points, reduces exposure to $< 50\%$ of that used during previous acquisition protocols. The incident flux was reduced to minimize damage while still providing adequate spectral resolution (the mechanism to reduce flux involves masking prior to the grating which reduces the grating illumination and, if done excessively, leads to degradation of the spectral resolution). With these improvements, our implementation of X-PEEM to these biomaterials studies has evolved to the point where radiation-sensitive systems such as PMMA can be measured with minimal artifacts.

3. Data Analysis

3.1. Reference Spectra. The spectra of PS, PMMA, and human serum albumin (HSA) were recorded using scanning transmission X-ray microscopy (STXM) on free-standing thin films (PS, PMMA) or as a solvent-cast deposit on a silicon nitride window (HSA). The STXM energy scale was calibrated using the sharp C 1s \rightarrow Rydberg lines in CO₂.²⁹ The calibrated spectra were set to an absolute linear absorption scale by scaling

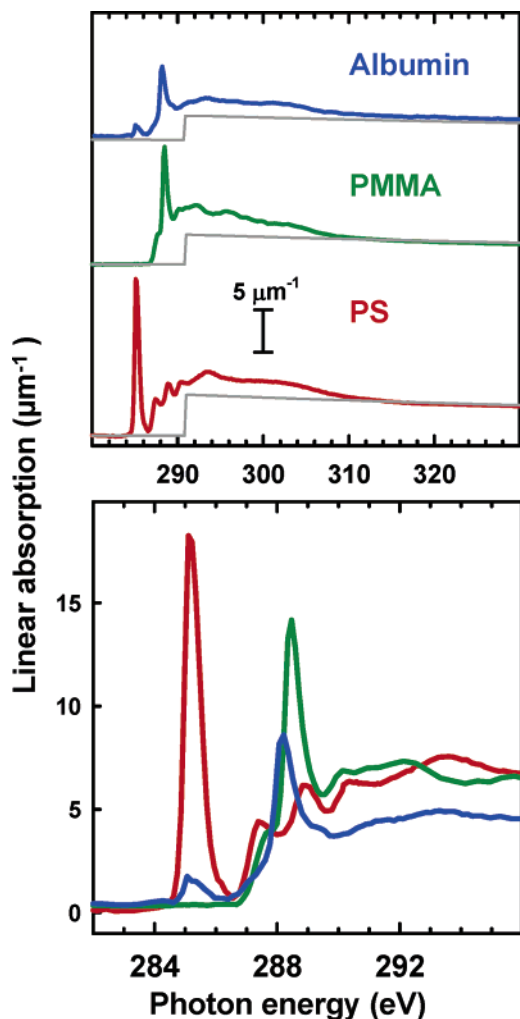


Figure 1. (a) C 1s X-ray absorption spectra of polystyrene (PS, red), poly(methyl methacrylate) (PMMA, green), and human serum albumin (HSA, blue) recorded from pure materials. The spectra are plotted on an absolute linear absorption scale (with offsets). The gray lines indicate the elemental response.³² (b) Expanded comparison of the near edge region.

to match the elemental response of 1 nm at bulk densities ($\rho_{\text{PS}} = 1.05$, $\rho_{\text{PMMA}} = 1.18$, $\rho_{\text{HSA}} = 1.0$ ³⁰), computed from standard tables of elemental X-ray absorption.^{31,32} These linear absorption spectra were the reference spectra used in fitting the C 1s image sequences of HSA-covered PS/PMMA. Although the energy resolution of STXM (0.1–0.2 eV) is better than that of X-PEEM (0.4–0.5 eV), the sharpest features in the X-PEEM spectra of the samples studied in this work have the same width as their counterparts in the STXM reference spectra due to the natural breadth of the peaks. Furthermore, as discussed in the next section, the recorded X-PEEM stacks are Io-normalized using corrections for systematic line shape distortions that would otherwise give different X-PEEM and STXM line shapes. For these reasons it is reasonable to use the STXM reference spectra for the analysis of the X-PEEM measurements.

Figure 1 presents the optical linear absorption spectra of pure PS, PMMA, and albumin thin films in the C 1s regions. The dark-gray lines are the computed elemental response.³² All three materials exhibit distinct C 1s spectra. The PS spectrum is dominated by the strong C 1s(C=C) $\rightarrow \pi^*_{\text{C}=\text{C}}$ transition at 285.1 eV. The albumin and PMMA spectra are each dominated by strong C 1s(C=O) $\rightarrow \pi^*_{\text{C}=\text{O}}$ transitions. However, the $\pi^*_{\text{C}=\text{O}}$ peak in albumin occurs at 288.20(6) eV, 0.25(8) eV below the $\pi^*_{\text{C}=\text{O}}$ peak in PMMA which occurs at 288.45(6) eV. The 0.25

eV energy shift is mainly associated with the change in energy of the C 1s level since the carbonyl carbon is in a less electronegative environment in the amide (R-CONH) than in the ester (R-COOMe). This shift is small but clear and has been documented previously.²⁴ It forms the basis for chemical differentiation of albumin (and other proteins) from PMMA (and other esters). In addition, the shape of the low-energy side of the $\pi^*_{\text{C}=\text{O}}$ peak is different in the two species. These differences assist differentiation of PMMA and albumin and thus the accuracy of the mapping is improved when longer range image sequences are used.

There are many factors in addition to the X-ray absorption coefficient that determine the signal strength from a given point on a surface, and thus the image contrast in X-PEEM. However, for a flat sample, with materials likely to have similar work function and similar scattering and propagation properties for low-energy electrons, and in the absence of any charging effects (all the case here), the X-ray absorption factor should dominate the response. Thus, although fully quantitative results require accurate information about the material dependence of sampling depth and electron propagation, we believe the approach used in this work, which uses quantitative reference spectra of the pure materials and a measured sampling depth, will give results for which the relative quantization of albumin on different parts of the surface is meaningful, and that the quantization will suffer at most from small systematic errors.

3.2. Chemical Mapping. Each image sequence was normalized to ring current and the I_0 signal from an HF etched Si wafer recorded under the same acquisition conditions. The I_0 signal was divided by the intrinsic X-ray absorption of Si³² and also by a linear energy term to account for the bolometric response function of this type of detection.³³ Since the energy scale of the ALS 7.3.1 beamline can change significantly from day to day, each image sequence was carefully calibrated to set the position of the peak of the (asymmetric) C 1s $\rightarrow \pi^*_{\text{C}=\text{C}}$ transition of the PS domains to 285.15 eV.

The normalized image stack was analyzed using the “stack fit” routine³⁴ implemented in the analysis package, aXis2000.³⁵ This routine performs a least-squares fit to the spectrum at each pixel in an image sequence to a linear combination of the reference spectra of the pure materials, and to an additional “constant” (energy-independent) term. The fit coefficients are then assembled to form component maps which are maps of the spatial distribution of each component in the area imaged. Because the reference spectra are quantitative (the intensity scale of each one is the signal expected from 1 nm of the material at bulk density), the intensities of the component maps are correct relative to each other. To give an absolute “thickness” scale to the component maps, it is necessary to set the scale for the total thickness. This is estimated to be 10 nm, based on the results of X-PEEM measurements of a series of pure PS thin films of varying thickness.²⁸ In the case of the albumin map it is important to note that thickness is “quantized” by the finite size of the molecule. If albumin is aligned with its smallest dimension (4 nm) normal to the surface, a thickness of 1 nm in a given region should be interpreted as one-fourth of the surface of that region being covered by a monolayer of albumin while the other three-fourths of the region is bare. Effectively, the thickness scale for the albumin component can be re-interpreted as a coverage scale, with a value of 4 nm representing saturated monolayer coverage.

As an example of this process, the results from a stack fit analysis of the C 1s X-PEEM data for albumin adsorption from a 0.005 mg/mL solution for 20 min are presented in Figure 2

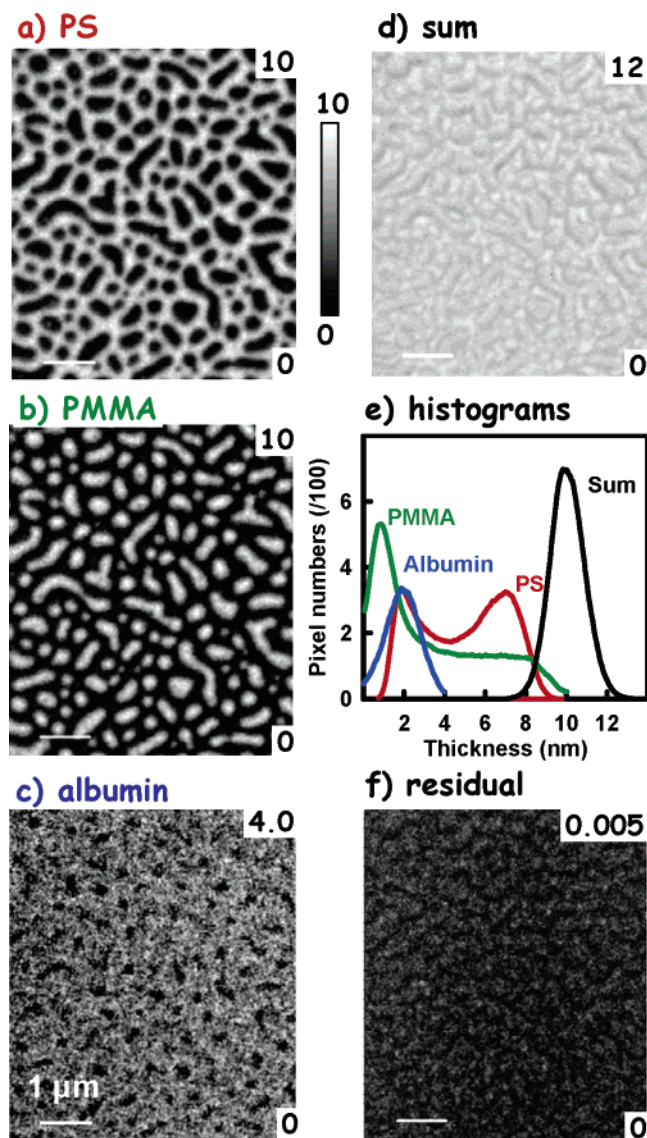


Figure 2. Component maps of (a) PS, (b) PMMA, and (c) albumin for a PS/PMMA blend substrate exposed to a 0.005 mg/mL HSA aqueous solution for 20 min, derived from pixel-by-pixel curve fits of a C 1s image sequence. The numbers in the upper and lower right of each component map are limits of the thickness gray scales in nm. (d) Sum of the PS, PMMA, and albumin thickness component maps. (e) Histograms of the component and sum maps. The narrow distribution of the sum supports our assumption of similar work function and sampling depth for the various surface regions (PS, PMMA, and interface). The average value of the sum was set to 10 nm to set the thickness scale. (f) Map of the residual of the fit. The gray scale in the latter case is the deviation of the fit and the measured signal, averaged over all energies.

in the form of maps of each component: (a) PS, (b) PMMA, (c) albumin, as well as (d) the sum of these components, (e) histograms of the thicknesses for each component and the sum, and (f) the residual of the fit. The grayscale limits are the minimum and maximum thickness per pixel. Lighter intensities indicate locations where there is more of that component. The thickness values were obtained by normalizing the sum of all three component map signals to the estimated total sampling depth of 10 nm. Note that the summed signal (Figure 2d) is quite constant over the field of view, with a variation of about 15%. This supports our assumption that the sampling depth is similar in the chemically different regions. The component maps show that the PS domains are continuous and the PMMA domains are discontinuous, as found in previous studies of PS/

PMMA blends prepared from high MW PS and PMMA.²³ At neutral pH, the HSA molecule has a size of $\sim 4 \times 4 \times 14$ nm in its folded form. Surface plasmon resonance studies of albumin adsorbed on a pure polystyrene surface³⁶ have been interpreted in terms of a preferred adsorption geometry with the albumin molecule aligned with its long axis parallel to the surface. Thus, the albumin thickness values of < 4 nm found for all of the surfaces studied in this work correspond to adsorption at less than one monolayer. This is also consistent with radio-labeling results from similar preparations.³⁷

Figure 3a displays a color-coded composite map, which reveals the spatial correlation of the chemical components. This is obtained by combining the component maps of PS, PMMA, and albumin, with the PS signal in red, the PMMA signal in green, and the HSA signal in blue. In Figure 3a the intensity scale for each color is set so that the full range of each component is mapped to the full 0–255 range. Note that, to see details more clearly, Figure 3 displays only the central $17 \mu\text{m} \times 17 \mu\text{m}$ region of the full image shown in Figure 2. The color-coded map shows a distinct blue band at the interface between the PS and PMMA domains. The discontinuous PMMA domains are turquoise rather than green, indicating the presence of HSA on their surface, while the continuous PS domains are purple, indicating significant HSA also on the PS domains. Fibrinogen was also found to show interface preference when it adsorbed on to similar PS/PMMA substrates from unbuffered aqueous solutions.²⁴

To obtain the amount of albumin on different regions, signals specific to the PS and PMMA domains were extracted by using threshold masking of the component maps to select only those pixels where the signal was above a defined threshold. The interface signal from a ~ 80 nm band at the PS–PMMA interface was obtained by selecting those pixels not present in either the masked PS or masked PMMA maps. The amount of each component (PS, PMMA, and albumin) in each region [PS, PMMA, and interface] was then obtained by fitting the extracted spectrum using the same reference spectra used in generating the component maps by the stack fit. Figure 3b displays the masks while panels (c–e) of Figure 3 display the curve fit to each extracted spectrum. The intensities in these spectra are those obtained after adjusting the spectral intensity scale by the same factor which gave a thickness of 10 nm for the average of the sum of the component maps. The points with estimated uncertainties are the experimental spectra. The dark solid curves are the fits to the masked experimental spectra and the color curves are the weighted reference spectra. The results of these fits are reported in Table 1.

3.3. Histogram Analysis of the Albumin Distributions. To further investigate the changes in albumin thickness on the different regions with changes in concentration and exposure times, the albumin maps were segmented into three regions [PS, PMMA, and interface] and then histograms of those signals were derived. The same masks of the PS, PMMA, and PS/PMMA interface regions used to extract the spectra subjected to the curve fit were used to subdivide the albumin component map into three parts—albumin-on-PS, albumin-on-PMMA, and albumin-on-interface—by taking the product of the albumin component map with each mask. The histograms of each of those spatially segregated albumin signals are presented and discussed in the Results section.

3.4. Verification of Precision and Accuracy. Since the contributions of the albumin signal to the total signal are small and the changes in the amounts of absorbed HSA with exposure conditions are relatively even smaller, to build confidence in

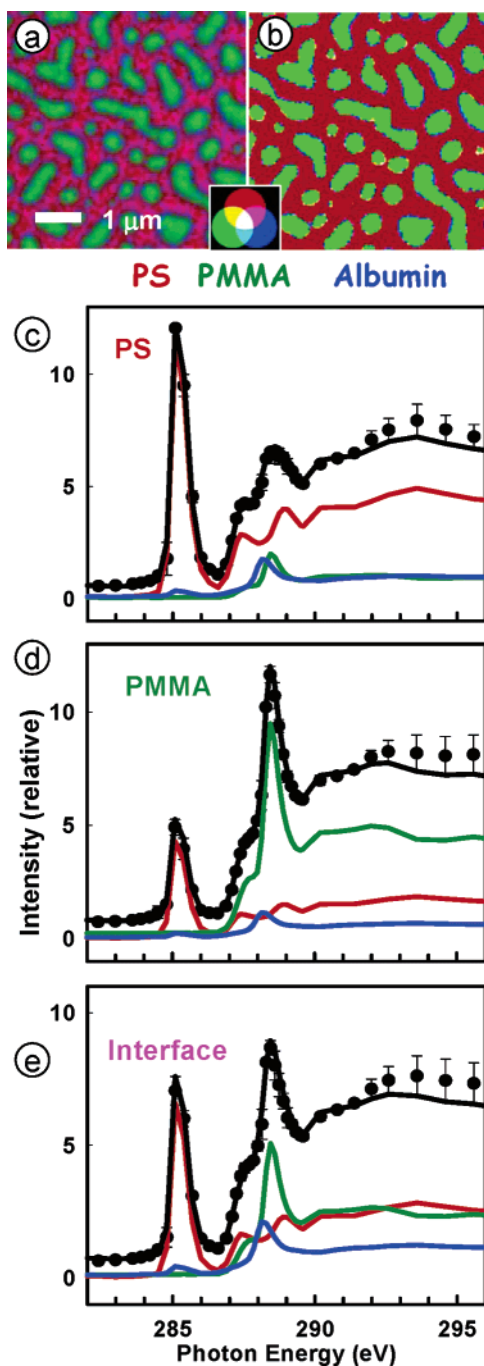


Figure 3. (a) Color-coded component map (left top, rescaled) for the (0.005 mg/mL, 20 min) albumin-covered PS/PMMA blend sample. The color wheel which allows the viewer to determine the composition in mixed regions. (b) Masks used to extract spectra of specific regions. [red = PS > 4 nm, green = PMMA > 4 nm, blue = PS/PMMA interface (all pixels not identified in the masks of the PS and PMMA domains)]. (c–e) Curve fits to the average C 1s spectra extracted from the masked regions (data, points; fit, thick solid line; components, thin lines).

our results, we carefully examined the various steps used to optimize the analytical methodology.

First, at least two measurements were made for each of the adsorption conditions. To minimize the radiation damage, each measurement was performed on a fresh area. The albumin distributions derived from the repeat results were in agreement within the estimated uncertainties.

Second, the spatial distribution of albumin on the surface has also been evaluated by measuring the N 1s edge. The N 1s signal

is a good indicator of the amount of albumin present since albumin is the only species with a N 1s signal. However, the N 1s signal is much weaker than the C 1s signal, and thus the N 1s edge is less sensitive than the C 1s edge for quantitative measurements. In addition, the N 1s signals do not give a specific measure of the PS and PMMA components of the substrate, although the morphology is readily visible due to the differences in elemental composition of PS and PMMA. The N 1s results (not shown in this work) are generally in agreement with those from the C 1s edge, especially in terms of trends, but there are some quantitative disagreements. Given that the C 1s signal has a balanced sensitivity to all three chemical components, we have chosen to present only the C 1s results. We are still exploring how to improve the accuracy and reliability of the N 1s measurement. We are also exploring how to optimize O 1s edge measurements as an additional source of chemical mapping information. PS is spectroscopically silent at the O 1s edge, and the radiation damage rate is higher at the O 1s edge than the C 1s edge. Thus, of the three possible edges, the O 1s edge provides the least specific and most unreliable information about this particular system.

Third, in addition to the threshold masking technique described in the preceding paragraph, which provides a convenient “single number” evaluation of spatial distributions, the spatial distributions on the three chemically distinct regions of the sample were characterized by examining the histograms of pixel values of albumin thickness. The method was described in detail in the previous section. Here, we note that these distributions are broad relative to the mean thickness. This width reflects the distribution of albumin thicknesses and not the statistical uncertainty. When the spectra from a grouping of pixels at a particular thickness level are selected, and the spectrum of each of those pixels is analyzed independently, the standard deviation of the derived albumin thickness from those repeat analyses is of the order of 0.1 nm, whereas the histogram peaks have widths (fwhm) of the order of 1.5 nm.

Fourth, there are a number of parameters in the analysis which can potentially affect the results. These include choice of fitting method (stack-fit versus SVD³⁴), the fine details of the reference spectra used (e.g., from PEEM versus from STXM, compensation for differences in energy resolution of PEEM versus STXM, elimination of small effects of radiation damage in the reference spectra, etc.), and the energy range of the spectral data employed (ideally, one wants to have as many energies where the X-ray absorption of the components differ substantially, but relatively few energies where the X-ray absorption of the components is the same; however, if too few energies are used, the statistical quality is reduced). All these factors were investigated in considerable detail. All reasonable choices gave similar quantitative results, and the same qualitative trends. The results presented herein represent the best choice of methodology, which is based on an extensive exploration of a complex and highly coupled parameter space.

In summary, we believe these results and the estimated errors cited represent a “best case” analysis. Clearly, systematic errors are possible. For example, if one changed the depth to which the total thickness is normalized, the amounts of protein would change in proportion. We justify the choice of 10 nm as the *total* depth contributing to the measured signal because the sampling depth for PS (thickness for which the signal drops by 1/e) has been measured to be 4 ± 1 nm.²⁷ As is typical of systematic errors, selection of a different value to normalize the total thickness would change the reported albumin thicknesses by an amount larger than our estimated precision.

TABLE 1: Concentration Dependence of Adsorption of HSA on PS/PMMA from De-ionized Water Solution: Composition of PS, PMMA, and PS/PMMA Interfaces (Uncertainty: ± 0.1 nm^a)

region	composite (nm/pixel)	0.005 mg/mL		0.01 mg/mL		0.05 mg/mL	
		fit ^b	hist. ^c	fit	hist.	fit	hist.
PS region	PS	6.5		6.5		5.8	
	PMMA	1.4		1.3		1.6	
	albumin	2.1	2.1	2.2	2.2	2.6	2.6
PMMA region	PS	2.3		1.9		2.3	
	PMMA	6.4		6.7		5.6	
	albumin	1.3	1.3	1.4	1.4	2.1	2.1
interfacial region	PS	3.8		3.7		3.7	
	PMMA	3.7		3.7		3.5	
	albumin	2.5	2.5	2.6	2.6	2.8	2.8
ratio (alb. on PS/PMMA/interface)		1.6/1.0/1.9		1.6/1.0/1.9		1.2/1.0/1.3	

^a See text. ^b Results from curve fit. ^c Centroid of the albumin distribution histograms. See text.

However, such errors affect the scale, not the qualitative trends with changes in adsorption conditions, and it is the latter we stress in the rest of this presentation.

4. Results

4.1. Concentration Dependence of Albumin Adsorption.

The adsorption of albumin from deionized water solutions was studied at three different concentrations: 0.005, 0.01, and 0.05 mg/mL, in each case for a fixed exposure time of 20 min. Figure 4 presents the color-coded composite maps for these three systems, derived from stack fits of C 1s image sequences. The maps on the left are not rescaled, which means a common thickness scale (min/max over all three components) is used for all three components. The maps on the right are rescaled, which means that the intensity of each color is adjusted to fill the full scale of the associated component map. The nonrescaled maps show there is a small but systematic increase in the amount of albumin adsorbed on the surface with increasing albumin concentration. The rescaled maps better show how the spatial distribution of the albumin changes with increasing concentration.

As the albumin concentration increases, the nonrescaled maps show that the color of the continuous PS domains changes from “red rather than purple” to “purple rather than red” and the discontinuous PMMA domains also change from pure green to a more turquoise color. These results show that the thickness of albumin on both the PS and PMMA domains increases with concentration. The rescaled maps clearly show that the interface of the PS and PMMA remains blue in all three cases. These results indicate that, under these adsorption conditions, the preferred adsorption site of albumin is the PS/PMMA interface.

Using the component map masking technique described above, spectra of the PS, PMMA, and interface were extracted and fit to obtain the relative amount of each component in each region. Table 1 presents the results of this quantitative analysis. There is around 15–20% PMMA in the masked PS region and 20–25% PS in the masked PMMA region, which is associated mostly with microdomains.²³ The interfacial region contains about the same amount of PS and PMMA, as expected from the spatial location. What interests us most is the amount of albumin on the chemically different regions of the surface. These values are highlighted in Tables 1 and 2 in bold. The last row of Table 1 shows the ratio of albumin on different regions for the three concentrations studied. This analysis is consistent with the qualitative information in the color-coded maps (Figure 4). The preferred site of albumin adsorption at lowest concentration (0.005 mg/mL) is the PS/PMMA interface, which implies this

is the one with a kinetic or thermodynamic advantage relative to adsorption on the PS or the PMMA domains. The albumin thickness at the PS/PMMA interface increased by only 0.3 nm as the concentration was increased from 0.005 to 0.05 mg/mL, suggesting these sites get saturated at very dilute conditions. Albumin shows a stronger preference for PS domains than for PMMA domains at all three concentrations but the preference gets smaller with increasing concentration. The albumin thickness on the PS domains remains almost the same as the concentration changes from 0.005 to 0.01 mg/mL, but increases by 0.4 nm from 0.01 to 0.05 mg/mL. The albumin thickness on the PMMA domains also remains almost the same as the concentration changes from 0.005 to 0.01 mg/mL while it increases by 0.7 nm as the albumin solution concentration is increased from 0.01 to 0.05 mg/mL. Table 1 also shows that as the albumin amount increases, the strength of the PS signal decreases. This is consistent with the fixed sampling depth and thus the blocking of electrons from ionization of the polymer substrate by the overlayer of adsorbed protein.

Figure 5 plots the histograms of albumin distributions on different regions—PS, PMMA, and the PS/PMMA interfaces—for the three different concentrations. Each curve shows a Gaussian-like distribution. The centroids of the histograms are listed in Table 1. These numbers are very similar to the average of the albumin thickness from the curve fit, as expected. The widths of the distributions reflect the stochastic nature of the adsorption process, which means that various areas of each domain type are not covered equally. When the spectra from individual pixels with similar values on each histogram curve are isolated and curve fit, the variation in the thicknesses from those fits is of the order of 0.1 nm, which is the basis for our estimated statistical precision reported in the tables.

4.2. Exposure-Time Dependence. The adsorption of albumin from 0.01 mg/mL deionized water solutions was also studied for three different exposure times: 5, 20, and 60 min. The results for 20 min adsorption from 0.01 mg/mL albumin solution are the same as those in the previous section. We show the result here again in order to give a systematic description of exposure-time dependence. The (rescaled) color-coded maps of the three different exposure times are presented in Figure 6. In this case, the color of the discontinuous PMMA domains changes dramatically from pure green to green-blue and even turquoise in some locations. In the case of the 5 min exposure, the strong blue signal in the color composite map is located at the PS/PMMA interfaces but the blue at the interface becomes lighter with increasing exposure time.

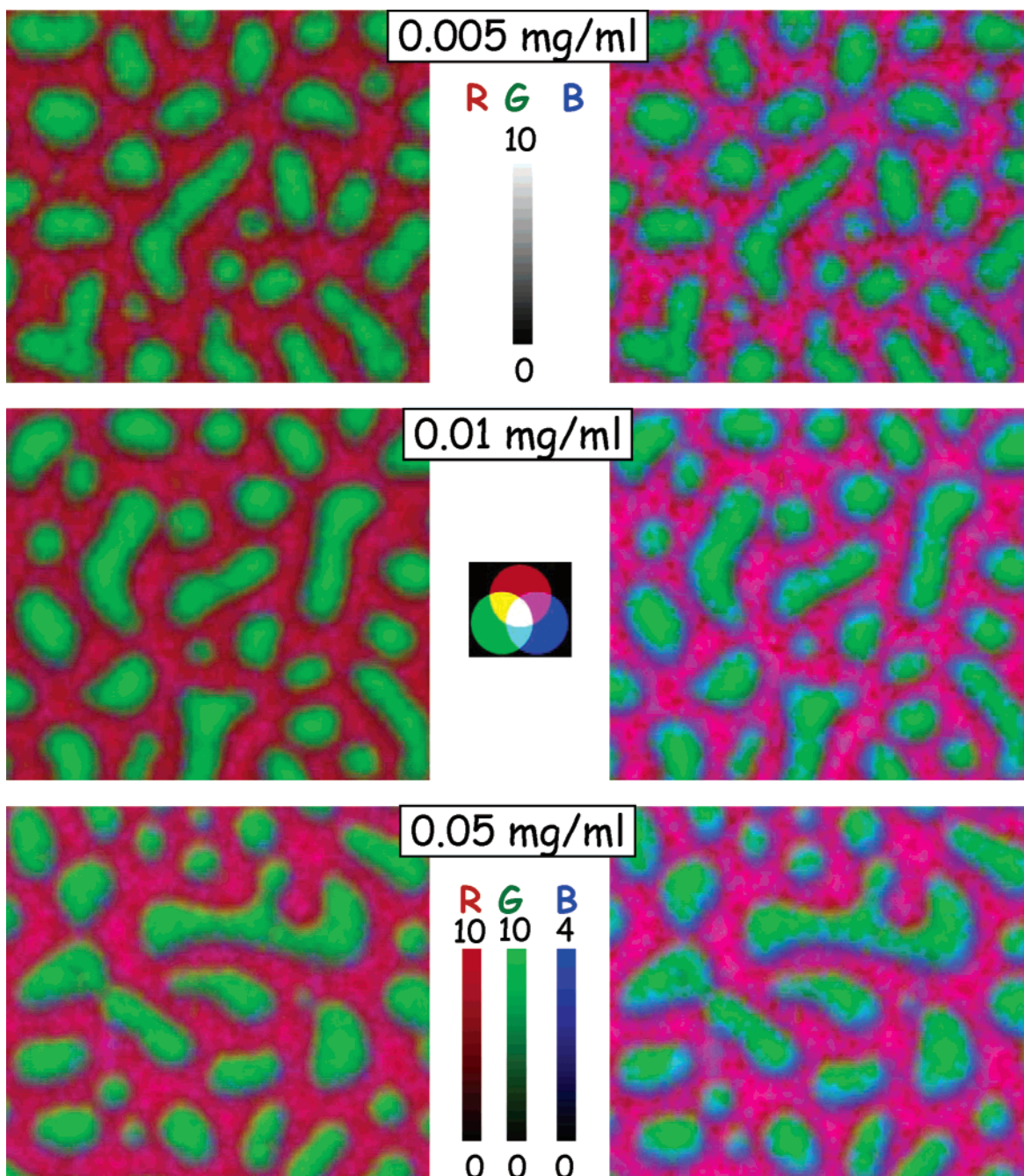


Figure 4. Concentration dependence (0.005, 0.010, and 0.050 mg/mL) of albumin adsorption on PS/PMMA: Color-coded component maps of albumin-covered PS/PMMA for the indicated solution concentrations and an exposure time of 20 min. (left) Nonrescaled maps on a single thickness scale for all three colors indicated by the upper scale; (right) rescaled maps with thickness limits as indicated by the lower intensity scales. The size of each image is $10 \mu\text{m} \times 10 \mu\text{m}$.

The results from curve fits to the extracted PS, PMMA, and interface spectra are shown in Table 2. These verify the trends presented visually in the color-coded composite maps of Figure 6. Similar to the concentration-dependence study, there is around 20–30% PMMA in the masked PS region and around 20–30% PS in the masked PMMA region due to micro domains.²³ In the case of the 5 min exposure, albumin has a very strong preference for PS and PS/PMMA interfaces. This indicates that the first sites of adsorption are the PS/PMMA interfaces at short exposure times, consistent with the result of the 20 min adsorption from dilute albumin solution. The albumin thickness on the PS domains increases slightly from 5 to 20 min and then remains the same after 20 min. This suggests that adsorption onto the PS domains saturates in less than 20 min. The thickness of albumin on the PMMA domains increases dramatically from

near zero at 5 min to 1.4 nm at 20 min and still keeps increasing to 1.9 nm at 60 min. This suggests that adsorption of albumin on the PMMA domains requires a longer time to saturate than that on the PS domains. The albumin thickness on the PS/PMMA interfaces shows a maximum of 3.0 nm for 5 min exposure but then decreases to 2.6 nm after 20 min, with no further change at longer exposure times.

Figure 7 plots the histograms of the albumin distributions on the different regions—PS, PMMA, and the PS/PMMA interfaces—for the three different exposure times. Each curve follows a quasi-Gaussian distribution except the histograms of albumin distributions for 5 min adsorption, where the albumin distribution on the PMMA domains follows a decaying linear curve and a peak is not observed. The average albumin thickness on the PMMA domains is nearly zero. The albumin distributions

TABLE 2: Exposure-Time Dependence of Adsorption of HSA on PS/PMMA from De-ionized Water Solution: Composition of PS, PMMA, and PS/PMMA Interfaces (Uncertainty: $\pm 0.1 \text{ nm}^a$)

region	composite (nm/pixel)	5 min		20 min		60 min	
		fit ^b	hist. ^c	fit	hist. ^c	fit	hist. ^c
PS region (nm/ pixel)	PS	5.8		6.5		4.9	
	PMMA	2.3		1.3		2.9	
	albumin	1.9	1.9	2.2	2.2	2.2	2.2
PMMA region (nm/pixel)	PS	2.6		1.9		2.7	
	PMMA	7.2		6.7		5.4	
	albumin	0.2	d	1.4	1.4	1.9	1.9
interfacial region (nm/pixel)	PS	3.5		3.7		3.7	
	PMMA	3.5		3.7		3.7	
	albumin	3.0	3.0	2.6	2.6	2.6	2.6
ratio (alb. on PS/ PMMA/interface)		9/1.0/15		1.6/1.0/1.9		1.2/1.0/1.4	

^a See text. ^b Results from curve fit. ^c Centroid of albumin distribution histograms. ^d No peak in the histogram.

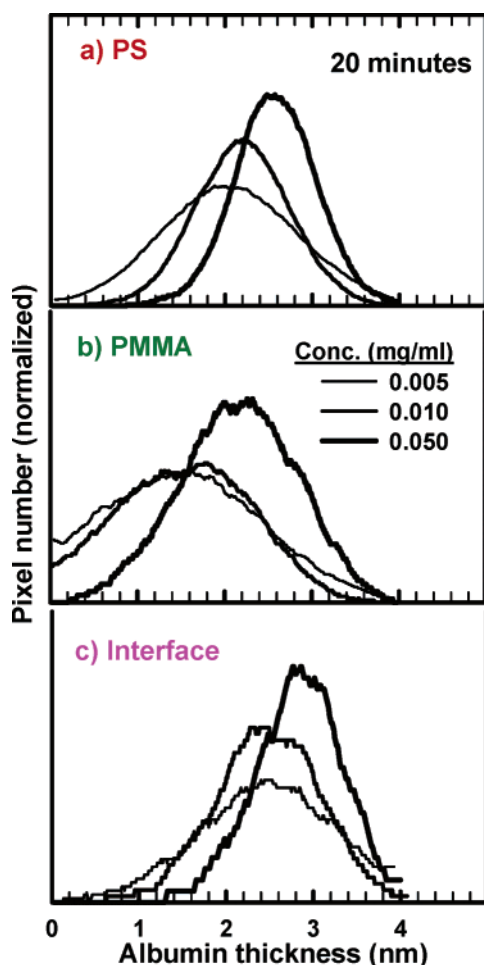


Figure 5. Histograms of the thickness of albumin thickness on different regions for adsorption for 20 min from solutions of concentrations of 0.005, 0.01, and 0.05 mg/mL. (a) Albumin on PS, (b) albumin on PMMA, and (c) albumin on the interface. The sum of pixels for each region for each exposure condition was set to a common value to take into account the fact that differently sized regions were imaged in the various samples.

on the PS and PS/PMMA domains for 5 min exposure have long tails into the thicker albumin region. The centroids of the histograms are listed in Table 2 as an alternate estimate of the average albumin thickness.

5. Discussion

The major finding of this study is that the preferred first site of albumin adsorption (at short time and low concentration) on

micro phase-separated PS/PMMA blends is the domain boundary, which we refer to here as the interface between the domains (our limited lateral spatial resolution precludes exact identification of the location of the albumin within the domain boundary region). At longer exposures, there is a redistribution of the protein away from the interfaces and toward the PS and PMMA domains (especially the PS domains). These trends, based on the data in Tables 1 and 2, are presented in Figure 8 in the form of log–log plots. As can be seen, the plots in Figure 8a are linear, thus suggesting in the case of the concentration dependence that adsorption on the different surface regions follows the Freundlich isotherm model.³⁸ Adsorption on the PS domains appears to achieve equilibrium quickly as indicated by the very small variation in albumin coverage with either concentration or exposure time. As seen in Figure 8b, adsorption to the interface at 0.01 mg/mL decreases and adsorption to the PMMA domains increases with time. Indeed, the form of the time variation suggests that there may be exchange of protein between these two regions. The reversibility of albumin adsorption on the PS/PMMA interfaces indicates that adsorbed albumin molecules are not denatured. Why does this initial localization and subsequent redistribution happen? Clearly, the answer to this question depends on the mechanisms of adsorption that are in play, and their dependence on the surface properties of both the protein and the adsorbing surface.

Globular proteins, including albumin, consist of hydrophobic (nonpolar) and hydrophilic (polar, charged) regions, and thus can engage in multiple mechanisms of adsorption including hydrogen bonding, electrostatic interactions, and hydrophobic interactions. Norde and Lyklema³⁸ have discussed these mechanisms and the driving forces behind them. Hydrophobic interactions play a major role in protein–surface systems; these are driven by entropy gain due to loss of structured water at the interacting surfaces, and conformational re-ordering. Examples where the adsorption is endothermic and/or where protein and surface have net charge of the same sign are common. In an aqueous environment, a protein adopts conformations where the hydrophilic (polar, charged) amino acid residues tend to be located externally and the hydrophobic residues located internally. However, not all of the hydrophobic groups are “hidden” in the interior and not all of the hydrophilic groups are exposed externally to water.³⁹ Thus, proteins in aqueous solution tend to have both hydrophobic and hydrophilic patches on the exterior surface, although the surface must be predominantly hydrophilic (or have a sufficient charge density) if the protein is to remain molecularly dispersed.⁴⁰

Given the amphipathic character of proteins as described, it is perhaps not surprising that albumin prefers to locate initially

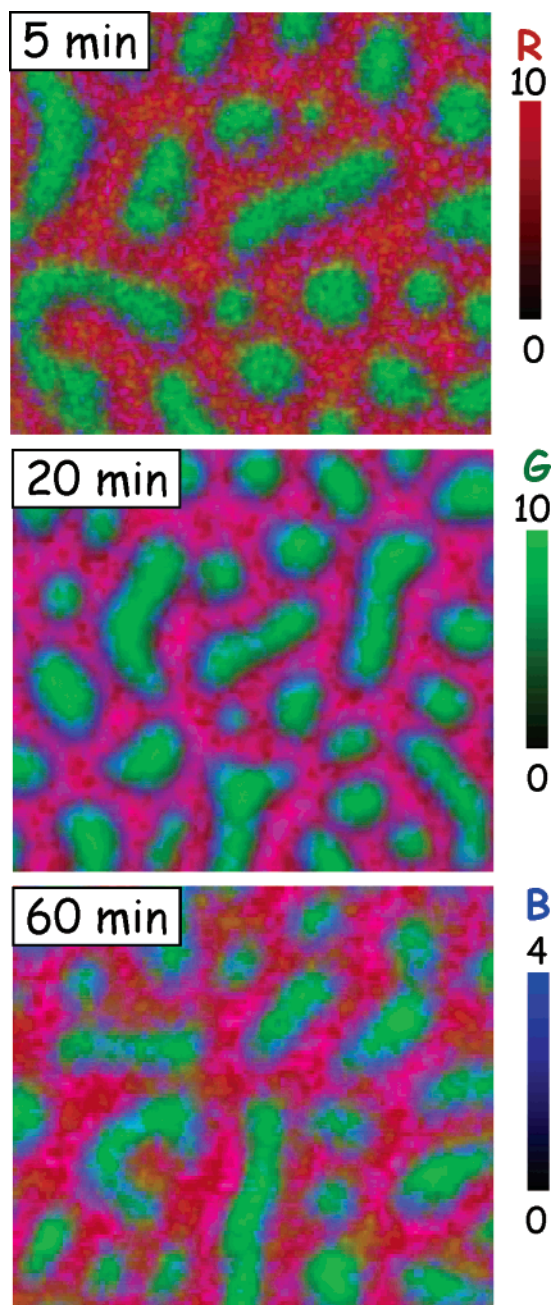


Figure 6. Exposure-time dependence (5, 20, and 60 min) of albumin adsorption on PS/PMMA: Color-coded component maps of albumin-covered PS/PMMA for the indicated times of exposure to an HSA solution of 0.01 mg/mL. Only rescaled maps are displayed, with thickness limits as indicated. The size of each image is $10 \mu\text{m} \times 10 \mu\text{m}$.

at the boundaries of the PS and PMMA domains. The difference in surface energy between PS and PMMA is significant as indicated by water contact angles of 97° and 76° ,⁴¹ respectively. Thus, the more hydrophobic regions of albumin should tend to bind to the PS domains while the more hydrophilic regions should bind to the PMMA domains. This preference is most easily accommodated by adsorption at the interfaces, as found here.

As the surface fills, sites which are kinetically most accessible, and/or those of lowest free energy, will be occupied first. In the present case the preferred interfacial locations will at some point be fully occupied and further adsorption will, perforce, occur on the domain surfaces. From the data at short time and low albumin concentration it appears that the more hydrophobic

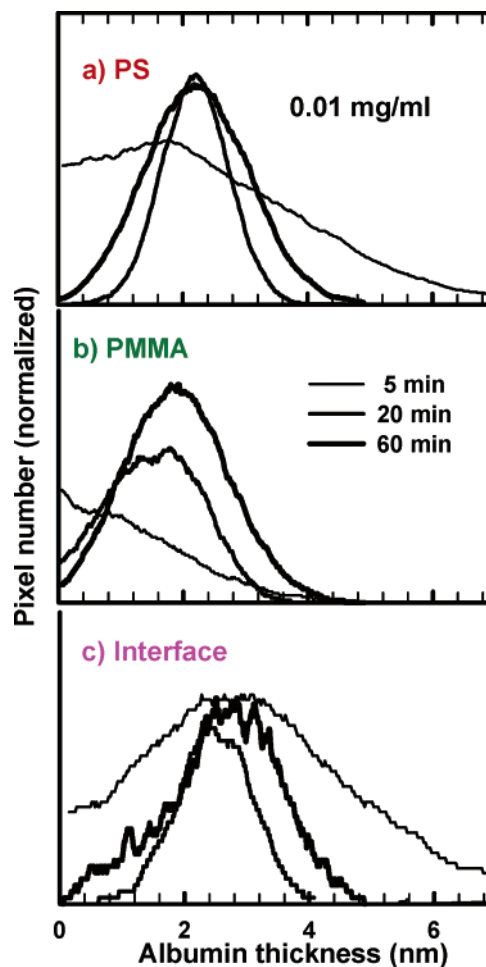


Figure 7. Histograms of the albumin thickness on different regions for adsorption from a 0.01 mg/mL solution for exposure times of 5, 20, and 60 min. (a) Albumin on PS, (b) albumin on PMMA, and (c) albumin on the interface. The sum of pixels for each region for each exposure condition was set to a common value to take into account the fact that differently sized regions were imaged in the various samples.

PS domains are favored initially over the PMMA domains, thus suggesting that the hydrophobic interactions expected to predominate between PS and albumin provide greater binding energy than the interactions that occur when albumin adsorbs on PMMA. As well as hydrophobic interactions, the latter may involve hydrogen bonding between the carbonyls of PMMA and the amide nitrogens of albumin. Dipole–dipole interactions may also occur.

The redistribution of protein on the surface at higher concentrations and longer times involving an apparent net loss of protein from the interface regions is intriguing, though perhaps counter-intuitive. The driving force for such a process is not clear from an energy standpoint, but it suggests either that desorption/re-adsorption is taking place which results in redistribution of albumin over the surface, or redistribution is occurring by surface diffusion (not involving desorption) as has been shown in other systems.^{42,43} It might be possible to distinguish between these possibilities by investigating whether redistribution occurs if the protein solution is replaced with solvent after, say, an adsorption time of 5 min. If it does, then the diffusion rather than the desorption–resorption mechanism would be favored.

Other work on protein adsorption where surfaces of deliberately varied chemical composition have been investigated includes that of Elwing and others using hydrophobicity

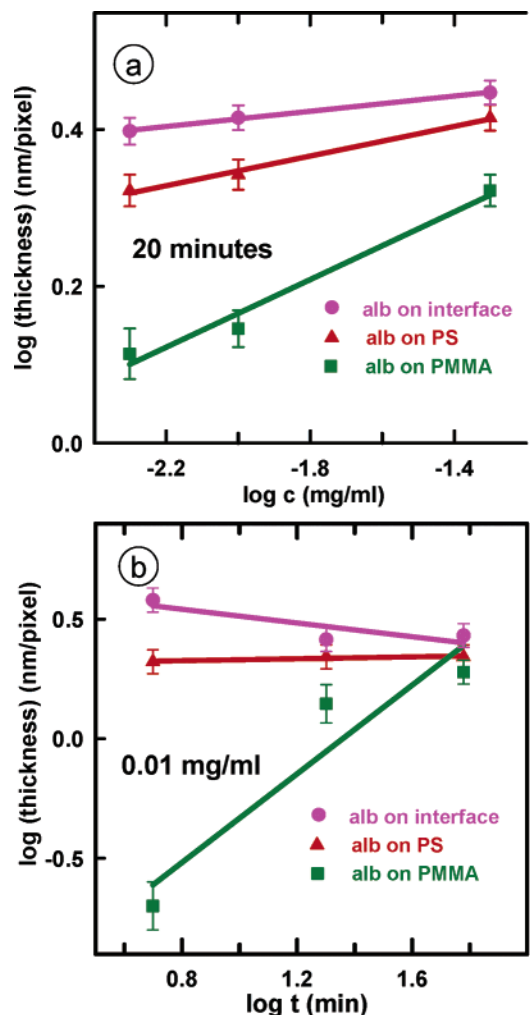


Figure 8. Log–log plots of the albumin thickness on the PS (red), PMMA (green), and PS/PMMA interface (pink) regions versus (a) concentration (for 20 min exposure time) and (b) exposure time (for adsorption from a 0.01 mg/mL solution).

gradients formed by differential deposition of silanes on silicon, to form a surface with a water contact angle which varied continuously from 90° to 10° along the length of the sample. In one study²⁰ it was shown that adsorption of fibrinogen from buffer and of proteinaceous material from plasma decreased monotonically from the hydrophobic to the hydrophilic end of the gradient, thus providing convincing evidence that proteins have stronger affinity for hydrophobic than for hydrophilic surfaces. In general the spatial resolution in these studies was of the order of 0.5 mm, 4 orders of magnitude lower than the ~80 nm spatial resolution of the present work.

A potential application of the X-PEEM methodology is to assist development of patterned polymer surfaces for microarrays and biochips which are being developed for rapid screening and high throughput analysis for proteomics and other applications.⁴⁴ Åsberg et al.⁴⁵ achieved hydrophobic patterning on a hydrophilic substrate with surface features of the order of 50 μm using polydimethyl siloxane (PDMS) stamping on a glass substrate. These surfaces were used to control the adsorption patterning of peptides and proteins. Interestingly, they allowed distinction between different conformations of the attached biomolecules. Bouaidat et al.⁴⁶ created patterns of protein adsorbing (glass) and nonadsorbing (PEO-like) areas using plasma polymerization combined with photolithography methods. Patterns with features of the order of 50 μm were achieved. In contrast to the work

reported in the present paper, none of this patterning work addresses the issues of differential adsorption kinetics and redistribution of protein over the surface as a function of time, although the latter may be important for biochip applications where the dimensional stability of protein arrays may be critical.

6. Summary

Albumin adsorption on a patterned PS/PMMA blend has been studied with X-PEEM at a spatial resolution better than 100 nm. The concentration and exposure-time dependence data are consistent with each other, showing that the preferred adsorption site at low concentration, and for short exposure, is the PS/PMMA interfacial region. We suggest that competition between polar and nonpolar interactions controls the first site of adsorption since it can be established on a short time scale. The X-PEEM results indicate there is reversible adsorption on the PS/PMMA interface. At longer exposure times, the system adopts a configuration in which the amount of albumin on the PMMA and PS domains increases significantly and there is a more even distribution over all three types of adsorption sites.

Acknowledgment. This research is supported by Natural Science and Engineering Research Council (NSERC, Canada) and the Canada Research Chair programs. X-ray microscopy was carried out using PEEM2 at the ALS. The ALS is supported by DoE under Contract DE-AC03-76SF00098.

References and Notes

- (1) Malmsten, M. *Biopolymers at interfaces*; Marcel Dekker: Basel, 2003.
- (2) Chittur, K. K. *Biomaterials* **1998**, *19*, 357–369.
- (3) Green, R. J.; Frazier, R. A.; Shakesheff, K. M.; Davies, M. C.; Roberts, C. J.; Tendler, S. J. B. *Biomaterials* **2000**, *21*, 1823–1835.
- (4) Sigal, G. B.; Mrksich, M.; Whitesides, G. M. *J. Am. Chem. Soc.* **1998**, *120*, 3464–3473.
- (5) Höök, F.; Kasemo, B. *Anal. Chem.* **2001**, *73*, 5796–5804.
- (6) Elwing, H. *Biomaterials* **1998**, *19*, 397–406.
- (7) Siedlecki, C. A.; Marchant, R. E. *Biomaterials* **1998**, *19*, 441–454.
- (8) Ta, T. C.; McDermott, M. T. *Anal. Chem.* **2000**, *72*, 2627–2634.
- (9) Kingshott, P.; StJohn, H. A. W.; Chatelier, R. C.; Griesser, H. J. *J. Biomed. Mater. Res.* **2000**, *49*, 36–42.
- (10) Lhoest, J.-B.; Wagner, M. S.; Tidwell, C. D.; Castner, D. G. *J. Biomed. Mater. Res.* **2001**, *57*, 432–440.
- (11) Mantis, D. S.; Ratner, B. D.; Carlson, B. A.; Moulder, J. F. *Anal. Chem.* **1993**, *65*, 1431–1435.
- (12) Ratner, B. D.; Horbett, T. A.; Shuttleworth, D.; Thomas, H. R. *J. Colloid Interface Sci.* **1981**, *83*, 630–642.
- (13) Sundgren, J.-E.; Bodo, P.; Ivarsson, B.; Lundstrom, I. *J. Colloid Interface Sci.* **1986**, *110*, 9–20.
- (14) Höök, F.; Rodahl, M.; Brzezinski, P.; Kasemo, B. *Langmuir* **1998**, *14*, 729–734.
- (15) Höök, F.; Kasemo, B. *Anal. Chem.* **2001**, *73*, 5796–5804.
- (16) Archambault, J. G.; Brash, J. L. *Colloids Surf B: Biointerfaces* **2004**, *33*, 111–120.
- (17) Castner, D. G.; Ratner, B. D. *Surf. Sci.* **2002**, *500*, 28–60.
- (18) Tirrell, M.; Kokkoli, E.; Biesalski, M. *Surf. Sci.* **2002**, *500*, 61–83.
- (19) Ostuni, E.; Chapman, R. G.; Liang, M. N.; Meluleni, G.; Pier, G.; Ingber, D. E.; Whitesides, G. M. *Langmuir* **2001**, *17*, 6336–6343.
- (20) Elwing, H.; Askendal, A.; Lundström, I. *J. Biomed Mater Res.* **1987**, *21*, 1023.
- (21) Gölander, C.-G.; Pitt, W. G. *Biomaterials* **1990**, *11*, 32–35.
- (22) Hitchcock, A. P.; Morin, C.; Heng, Y. M.; Cornelius, R. M.; Brash, J. L. *J. Biomater. Sci., Polym. Ed.* **2002**, *13*, 919–938.
- (23) Morin, C.; Ikeura-Sekiguchi, H.; Tyliczszak, T.; Cornelius, R.; Brash, J. L.; Hitchcock, A. P.; Scholl, A.; Nolting, F.; Appel, G.; Winesett, A. D.; Kaznacheyev, K.; Ade, H. *J. Electron Spectrosc.* **2001**, *121*, 203–224.
- (24) Morin, C.; Hitchcock, A. P.; Cornelius, R. M.; Brash, J. L.; Scholl, A.; Doran, A. *J. Electron Spectrosc.* **2004**, *137–140*, 785–794.
- (25) Peters, T., Jr. *All About Albumin: Biochemistry, Genetics, and Medical Applications*; Academic Press: New York, 1995.

- (26) Anders, S.; Padmore, H. A.; Duarte, R. M.; Renner, T.; Stammler, T.; Scholl, A.; Scheinfein, M. R.; Stöhr, J.; Séve, L.; Sinkovic, B. *Rev. Sci. Instrum.* **1999**, *70*, 3973–3981.
- (27) Jacobsen, C.; Wirick, S.; Flynn, G.; Zimba, C. Soft X-ray spectroscopy from image sequences with sub-100 nm spatial resolution. *J. Microsc.* **2000**, *197*, 173–184.
- (28) Wang, J.; Li, L.; Morin, C.; Hitchcock, A. P.; Doran, A.; Scholl, A. *J. Electron Spectrosc.*, in preparation.
- (29) Ma, Y.; Chen, C. T.; Meigs, G.; Randall, K.; Sette, F. *Phys. Rev. A* **1991**, *44*, 1848–1858.
- (30) Brandrup, J.; Immergut, E. H.; Grulke, E. A.; Bloch, D. *Polymer Handbook*; Wiley-Interscience: New York, 1999.
- (31) Henke, B. L.; Lee, P.; Tanaka, T. J.; Shimabukuro, R. L.; Fujikawa, B. K. *At. Nucl. Data Tables* **1982**, *27*, 1–256.
- (32) Henke, B. L.; Gullikson, E. M.; Davis, J. C. *At. Data Nucl. Data Tables* **1993**, *54*, 181–298.
- (33) Stohr, J. *NEXAFS Spectroscopy*; Series in Surface Science, Vol. 25; Springer: Berlin, 1992.
- (34) Hitchcock, A. P.; Morin, C.; Zhang, X.; Araki, T.; Dynes, J. J.; Stöver, H.; Brash, J. L.; Lawrence, J. R.; Leppard, G. G. *J. Electron Spectrosc. Relat. Phenom.* **2005**, *259–269*, 144–147.
- (35) aXis2000 is free for noncommercial use. It is written in Interactive Data Language (IDL) and available from <http://unicorn.mcmaster.ca/aXis2000.html>.
- (36) Green, R. J.; Davies, J.; Davies, M. C.; Robert, C. J.; Tendler, S. J. B. *Biomaterials* **1997**, *18*, 405–413.
- (37) Li, L.; Hitchcock, A. P.; Cornelius, C.; Brash, R. J., in preparation.
- (38) Norde, W.; Lyklema, J. *J. Biomater. Sci. Polym. Ed.* **1991**, *2*, 183–202.
- (39) Klotz, I. M. *Arch. Biochem. Biophys.* **1970**, *138*, 704–706.
- (40) Kuhn, L. A.; Swanson, C. A.; Pique, M. E.; Tainer, J. A.; Getzoff, E. D. *Proteins: Struct., Funct., Genet.* **1995**, *23*, 536–547.
- (41) Liu, Y.; Messmer, M. C. *J. Phys. Chem. B* **2003**, *107*, 9774–9779.
- (42) Axelrod, D.; Koppel, D. E.; Schlessinger, J.; Elson, E.; Webb, W. W. *Biophys. J.* **1976**, *16*, 1055–1069.
- (43) Cole, N. B.; Smith, C. L.; Sciaky, N.; Terasaki, M.; Edidin, M.; Lippincott-Schwartz, J. *Science* **1996**, *273*, 797–801.
- (44) Weibel, D. B.; Garstecki, P.; Whitesides, G. M. *Curr. Opin. Neurobiol.* **2005**, *15*, 560–567.
- (45) Åsberg, P.; Nilsson, K. P.; Inganäs, O. *Langmuir* **2006**, *22*, 2205–2211.
- (46) Bouaidat, S.; Berendsen, C.; Thomsen, P.; Guldager Petersen, S.; Wolff, A.; Jonsmann, J. *Lab Chip* **2004**, *4*, 632–637.